ACADEMIC PRESS

Available online at www.sciencedirect.com
SCIENCE DIRECT®

Journal of Catalysis 213 (2003) 235–240

JOURNAL OF CATALYSIS

www.elsevier.com/locate/jcat

Catalytic performance of $Cs_x(NH_4)_yH_zPMo_{12}O_{40}$ and related heteropolyacids in the methacrolein to methacrylic acid conversion: in situ structural study of the formation and stability of the catalytically active species

L. Marosi and C. Otero Areán *

Departamento de Química, Universidad de las Islas Baleares, 07071 Palma de Mallorca, Spain

Received 21 June 2002; revised 19 September 2002; accepted 23 September 2002

Abstract

The chemical and structural changes undergone by the Keggin-type compound $Cs(NH_4)_2PMo_{12}O_{40}$ with increasing time on stream under the conditions for methacrolein to methacrylic acid conversion have been studied by thermal analysis and in situ X-ray powder diffraction, which allowed the structure of the working catalysts and the changes involved in the catalyst ageing processes to be determined. The results show that, under the operating conditions of the catalytic reaction, restructuring of the $(PMo_{12}O_{40})^{3-}$ Keggin anion takes place, leading to formation of the reduced heteropolyanions $(PMo_{13}O_{41})^{-}$ and $(PMo_{14}O_{42})^{-}$. The six-electron reduced polyanion $(PMo_{14}O_{42})^{-}$ represents the end member of a series of catalytically active and thermally stable species which, by further reduction, decompose into catalytically less active MoO_3. Performance of catalysts derived from the above cesium-containing heteropolyacids is also compared to that of the anhydrous acid $H_3PMo_{12}O_{40}$ and of the anhydride $(MoO_x)_{0.5}(PMo_{14}O_{42})$ ($x \simeq 2$), for which a detailed structural analysis was carried out.

Keywords: Aging mechanism; $Cs(PMo_{13}O_{41})$; $Cs(PMo_{14}O_{42})$; Heteropolyacids; In situ XRD; Methacrolein; Methacrylic acid; Structure–activity relationship

1. Introduction

Heteropolyacids (HPAs) of the Keggin type, which combine strong Brønsted acidity with high redox activity, are known to be very effective catalysts for both acid-catalyzed and redox reactions [1,2]. A good example is the methacrolein (MA) to methacrylic acid (MAA) conversion, where HPAs of the type $Cs_xH_{3+y-x}PV_yMo_{12-x}O_{40}$ ($x = 0$–2, $y = 1$–2) are used as catalysts on an industrial scale [3,4]. However, a drawback of these catalysts is their relatively short lifetime under operating conditions [5,6]. Insufficient thermal stability of the catalytically active species is suspected to be the cause for long-term deactivation. The assumption that under working conditions the Keggin anion undergoes thermolysis, with formation of catalytically less active MoO_3, prompted several studies on the thermal stability of various HPAs and HPA salts [7–10]. In some of these studies, catalytic activity was correlated with formation of an anhydrous acid [6,11], but the existence of a catalytically active anhydride was also postulated [12–14] in the same context.

The structure of $H_4PVMo_{11}O_{40}$ under reaction conditions for the isobutyric acid to MAA conversion was studied by Ilkenhans et al. [11] by means of in situ X-ray diffraction (XRD). The authors conclude that under reaction conditions VO^{2+} cations are formed, and the resulting cubic vanadyl HPA salt was assumed to be an active phase in the catalytic process.

The effect of cesium-containing HPA salts on the selectivity and thermal stability of HPA catalysts for the oxidation of MA to MAA was studied by Mizuno et al. [15] and by Deußer et al. [16], and it was also mentioned in a patent application [17]. Recently, the structure of $CsH_2PMo_{12}O_{40}$ under reaction conditions for the MA to MAA conversion was studied by Marosi et al. [18] by means of in situ X-ray diffraction. It was found that decomposition of the cesium salt is not exclusively due to pure thermal stress. Under reaction conditions, a progressive migration of molybdenum

* Corresponding author.
E-mail address: dqueep0@clust.uib.es (C. Otero Areán).

0021-9517/02/$ – see front matter
doi:10.1016/S0021-9517(02)00078-7

from the Keggin units into the intracrystalline pore system of the solid takes place, and this diffusion process is essentially bound up with the nature of the redox catalytic reaction. The observed catalytic activity decline [18,19] was correlated with decomposition of the heteropolyacid and attendant formation of catalytically less active MoO_3.

However, despite the important insights derived from the above studies, the structural and chemical evolution of the working catalysts with increasing time on stream are not yet completely understood. The aim of this study was to carry out a more thorough elucidation of the structural changes to $Cs_x(NH_4)_yH_zPMo_{12}O_{40}$ compounds with increasing time on stream during MA to MAA conversion and of the chemical changes accompanying the catalyst aging process. $H_3PMo_{12}O_{40}$ and the new acid anhydride $(MoO_x)_{0.5}(PMo_{14}O_{42})$ are also considered.

2. Materials and methods

2.1. Sample preparation

$H_3Mo_{12}O_{40} \cdot xH_2O$ and $(NH_4)_3PMo_{12}O_{40}$ were obtained from Fluka. Samples of $Cs(NH_4)_2PMo_{12}O_{40}$ and $Cs_2(NH_4)PMo_{12}O_{40}$ were prepared by acidification of an aqueous solution of ammonium molybdate, phosphoric acid, and the appropriate amount of cesium nitrate with nitric acid. The resulting suspension was evaporated to dryness and the solid thus obtained was calcined at 653 K for 5 h. Further details on the preparation of these compounds were given elsewhere [18].

The anhydrous acid $H_3PMo_{12}O_{40}$ was obtained [20] by heating the hydrated $H_3PMo_{12}O_{40} \cdot xH_2O$ compound at 450 K in an electric furnace for 2 h. The new acid anhydride $(MoO_x)_{0.5}(PMo_{14}O_{42})$ was prepared [21] by calcining the ammonium salt $(NH_4)_3PMo_{12}O_{40}$ in an inert gas: about 5 g of the salt was heated in a vigorous nitrogen flow at 740 K for 2 h in a conventional flow reactor system, followed by cooling in a dessicator.

For catalytic tests, the above chemicals were tableted, crushed, and sieved to a mesh size of 0.2–0.4 mm.

2.2. Catalyst characterization and testing

Oxidation of MA to MAA was conducted under continuous flow conditions in the temperature range from 593 to 633 K. The in situ chamber used was a commercially available Parr high-temperature XRD cell which was modified to accommodate a special sample holder having a 5-ml catalyst bed volume and a newly designed heating system. In each experiment 5 g of catalyst were used. Feed composition and space velocity of the feed were 0.375 l MA, 1.27 l H_2O, 3.5 l air, and 2.82 l nitrogen per h. Further details on the catalytic chamber and setup for catalyst testing are given elsewhere [18,19].

Table 1
Surface area and pore volume of the catalysts

Catalyst	BET surface area (m^2/g)	Pore volume Hg-porosimetry (ml/g)
$H_3PMo_{12}O_{40}$	8	0.08
$(MoO_x)_{0.5}(PMo_{14}O_{42})$	6	0.23
$Cs(NH_4)_2PMo_{12}O_{40}$	5	0.24
$Cs_2(NH_4)PMo_{12}O_{40}$	3	0.25

Powder XRD patterns were obtained by using a Siemens D5000 theta/theta instrument and Cu-K_α radiation. The programs Win-Index, Win-Metric, and Win-Rietveld from Sigma-C GmbH (Munich) were used for analysis of the XRD patterns and for structure refinement. Computer simulation of the diffraction patterns was performed by using the Cerius^2 Crystallographic Software of Molecular Simulations Inc., Cambridge, UK.

Thermograms of the samples were obtained on a TA SDT 2960 thermal analyzer. Samples about 5 mg in weight were heated to 873 K in a platinum sample pan under a dry air or nitrogen flow at a constant heating rate of 10 K min^{-1}.

3. Results and discussion

3.1. Characterization of catalysts prior to exposure to methacrolein

The fresh catalysts were characterized by powder XRD, BET surface area (as measured by nitrogen adsorption at 77 K), and mercury porosimetry. Results on surface area and pore volume are give in Table 1. For $Cs(NH_4)_2PMo_{12}O_{40}$ and $Cs_2NH_4PMo_{12}O_{40}$ the corresponding XRD patterns, shown in Fig. 1 curves a and b, are coincident with those reported in the literature [22,23] and confirm that these compounds have the expected cubic Keggin-type structure. The diffraction pattern of the anhydrous acid $H_3PMo_{12}O_{40}$ (Fig. 1c) corresponds to a trigonal structure, which was recently described in detail elsewhere [20].

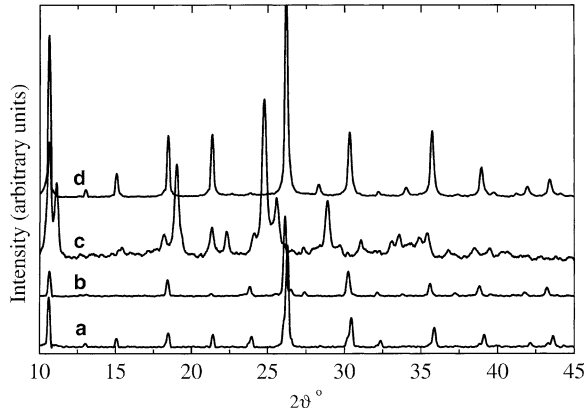

Fig. 1. X-ray diffraction patterns of (a) $Cs(NH_4)_2PMo_{12}O_{40}$, (b) $Cs_2NH_4PMo_{12}O_{40}$, (c) $H_3PMo_{12}O_{40}$, and (d) $(MoO_x)_{0.5}(PMo_{14}O_{42})$.

Table 2
X-ray powder diffraction data for $(MoO_x)_{0.5}(PMo_{14}O_{42})$

$2\theta_{obs}$	d_{obs}/Å	$(I/I_0)_{obs}$	$(I/I_0)_{calc}$	(hkl)
10.601	8.3379	65	59	011
12.992	6.8087	4	3	111
15.014	5.8960	11	9	002
18.416	4.8138	27	27	112
21.294	4.1692	29	26	022
26.158	3.4039	100	100	222
28.293	3.1517	4	5	123
30.294	2.9479	36	36	004
32.199	2.7777	2	2	033
32.179	2.7794	2	2	114, 330
33.972	2.6367	5	5	024
35.683	2.5141	38	38	233
38.911	2.3127	14	15	015, 143
39.682	2.2695	2	2	115, 333
41.930	2.1529	6	6	125
43.373	2.0845	12	12	044
46.149	1.9654	11	10	006, 244
47.491	1.9129	10	9	116, 235
48.802	1.8645	2	2	026
49.450	1.8416	1	1	344
50.091	1.8195	6	6	145
51.356	1.7777	11	10	226
53.816	1.7020	3	3	444
55.021	1.6676	21	21	710, 055
56.202	1.6353	1	1	046
57.373	1.6047	9	8	336, 255
58.526	1.5758	1	1	246
61.905	1.4976	19	16	237
64.105	1.4516	13	11	147, 455

The new anhydride $(MoO_x)_{0.5}(PMo_{14}O_{42})$, prepared by calcining $(NH_4)_3PMo_{12}O_{40}$ in nitrogen as described above, gave the XRD pattern shown in Fig. 1 curve d. This diffractogram could be indexed by assuming a cubic unit cell, $a_0 = 1.1792$ nm, with the results shown in Table 2. Further structural characterization of $(MoO_x)_{0.5}(PMo_{14}O_{42})$ will be discussed after the formation process of this compound is considered.

3.2. Formation and structural analysis of $(MoO_x)_{0.5}(PMo_{14}O_{42})$

The solid product obtained by calcination of $(NH_4)_3PMo_{12}O_{40}$ at 740 K in a nitrogen atmosphere showed a deep bluish-black colour, which is characteristic of highly reduced molybdenum blue compounds [24]. Chemical analysis showed that it was free from ammonia. The chemical composition of the resulting product was inferred from the corresponding mass loss of 6.14% of the parent compound during calcination, as determined by thermogravimetry. This mass loss can be accounted for according to the following thermal decomposition process:

(a) $(NH_4)_3PMo_{12}O_{40} \rightarrow (NH_4)_{1.67}H_{1.33}PMo_{12}O_{40} + 1.33NH_3\uparrow$,

(b) $(NH_4)_{1.67}H_{1.33}PMo_{12}O_{40} \rightarrow H_8PMo_5^{5+}Mo_7^{6+}O_{40} + 0.835N_2\uparrow$,

(c) $H_8PMo_5^{5+}Mo_7^{6+}O_{40} \rightarrow (PMo_5^{5+}Mo_7^{6+}O_{36}) + 4H_2O\uparrow$.

The calculated weight loss for this process is 6.28%, in excellent agreement with the measured value of 6.14%.

The above thermal decomposition process is supported by temperature-programmed reduction (TPR) measurements [25,26], by IR spectroscopy [10], and by single-crystal structure analysis of $(NH_4)_3PMo_{12}O_{40}$ [27]. According to TPR results, thermal decomposition of the ammonium salt under an inert atmosphere occurs in a temperature range between 620 and 800 K with formation of NH_3, N_2, and H_2O, thus implying reduction of Mo^{6+} ions to a lower oxidation state. Analysis of IR spectra and single crystal XRD and TG data [28] led to the conclusion that in $(NH_4)_3PMo_{12}O_{40}$ there are two groups of NH_4^+ ions; those in one group are strongly bonded to the oxygen shell of the Keggin anions, while those in the other group are more weakly bounded. On calcination, ammonia is released from the weakly bounded NH_4^+ ions, leaving the corresponding number of Brønsted acid sites (step (a) above). Thermolysis of the strongly bounded NH_4^+ ions occurs in step (b), which implies oxidation to free dinitrogen and consequent five-electron reduction of the remaining HPA unit. Finally, water is lost in step (c), leading to the overall stoichiometry $PMo_{12}O_{36}$.

In order to further characterize the new anhydride obtained, we carried out structure determination by powder XRD using the Rietveld method. It should be pointed out, however, that the thermal decomposition product of $(NH_4)_3PMo_{12}O_{40}$ showed rather low crystallinity, which complicated structure refinement. For this reason, intensity calculation of the simulated diffraction patterns was performed using several tentative structure models by varying the fractional coordinates and occupancy factors of both molybdenum and oxygen atoms and also by moving molybdenum atoms from the Keggin unit into the intracrystalline pore system. Structure modeling showed that the measured XRD pattern could only be simulated in a satisfactory way when crystallographic sites in the close vicinity of the polyanion oxygen shell were partially occupied by molybdenum atoms lying outside the Keggin unit (see below). In this way we arrived at a Rietveld goodness-of-fit indicator $S = R_{wp}/R_{exp} = 1.22$, which implies a good concordance [29] between the calculated and the observed diffraction patterns; further details on the Rietveld analysis will be given elsewhere (Marosi et al., in preparation). Table 3 shows the resulting atomic coordinates and occupancy factors; the structure obtained is depicted in Fig. 2. This figure shows that the Keggin units are capped by two molybdenum atoms situated along the fourfold symmetry axis. It is also shown in Fig. 2 that the central PO_4 tetrahedron shares its oxygen atoms with four Mo_3O_{13} units consisting of three edge sharing MoO_6 octahedra. These four Mo_3O_{13} units are connected to one another by sharing corners, thus forming the α-Keggin cage. There are six cystallographically equivalent positions, located on the diagonal ends of the Keggin unit,

Table 3
Fractional atomic coordinates and stoichiometric occupancy factors (k) of the Mo, P, and O atoms in $(MoO_x)_{0.5}(PMo_{14}O_{42})$

Atom	x	y	z	k
P	0.75	0.75	0.75	1.00
Mo(1)	0.4668(1)	0.4668(1)	0.2581(3)	12.02(0.16)
Mo(2)	0.7606(15)	0.7386(15)	0.1000(8)	2.014(0.25)
Mo(3)	0.25	0.75	0.75	0.423(0.07)
O(1)	0.3260(13)	0.3260(13)	0.3260(13)	4.00(0.11)
O(2)	0.6520(9)	0.6520(9)	0.0167(19)	11.737(0.26)
O(3)	0.0651(10)	0.0651(10)	0.7653(18)	12.002(0.24)
O(4)	0.1259(10)	0.1259(10)	0.5462(18)	12.024(0.25)
O(5)	0.246(13)	0.7500(90)	0.246(13)	1.936(0.18)

favorable for further coordination of molybdenum atoms. The additional two molybdenum atoms, denoted as Mo(2) in Table 3, occupy two of these positions at both ends of a diagonal of the polyhedron, and each of them is coordinated to an extra oxygen atom (O(5) in Table 3) and four oxygen atoms of the Keggin unit. This yields an overall stoichiometry $PMo_{14}O_{42}$, which can be formally obtained (except for a small imbalance in phosphorus content) by multiplying the previous $PMo_{12}O_{36}$ formula by a factor of 1.17. Hence, on passing from the parent $(NH_4)_3PMo_{12}O_{40}$ salt to the $(MoO_x)_{0.5}(PMo_{14}O_{42})$ anhydride there is a six-electron reduction process. Note that the capped Keggin unit in Fig. 3 should bear a net electric charge close (or equal) to -1, which has to be balanced by a cationic species. In the above formula we wrote this cationic species as MoO_x, because the exact number of its oxygen atoms (which are located outside the Keggin unit) could not be determined; only the corresponding number of molybdenum atoms (Mo(3) in Table 3) is known. However, the analogous solid state transformation processes, with formation of VO_2^+ and VO^{2+} cations by migration of vanadium ions from the Keggin cages into the intracrystalline pore system and restructuring of the lacunary Keggin units were reported [11,23,30–32] for $(NH_4)_5PVMo_{11}O_{40}$ and $H_{3+x}PV_xMo_{12-x}O_{40}$ compounds. Therefore, it seems likely that in $(MoO_x)_{0.5}(PMo_{14}O_{42})$ the actual value of x is close to 2.

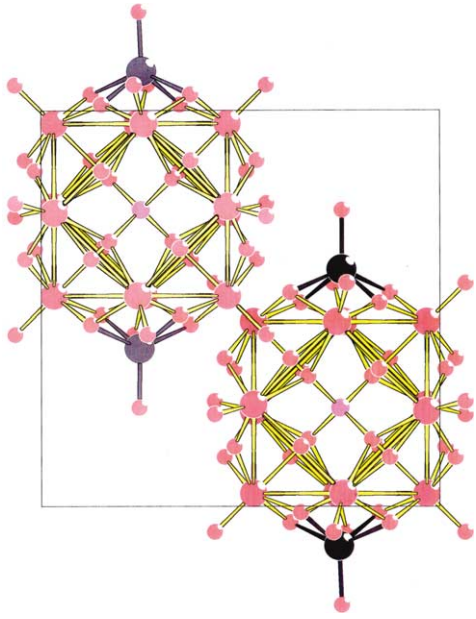

Fig. 2. Three-dimensional arrangement of the Keggin units and of the extraframework Mo(2) atoms in the structure of $(MoO_x)_{0.5}(PMo_{14}O_{42})$, viewed along the a-axis. The Mo(3) atoms (Table 3) are not shown.

Table 4
Comparison of catalysts performance in the MA to MAA conversion

Catalyst	Conversion (%)	Selectivity MAA (%)	Lifetime (h)[a]
$H_3PMo_{12}O_{40}$	36.4	50.2	ca. 15
$(MoO_x)_{0.5}(PMo_{14}O_{42})$	48	53	20–30
$Cs(NH_4)_2PMo_{12}O_{40}$	63.7	56	ca. 200
$Cs_2(NH_4)PMo_{12}O_{40}$	50.7	54	>380

[a] For the purpose of this work, lifetime is meant to indicate the turning point at which conversion and selectivity start to decrease, as seen in Table 5 for $Cs(NH_4)_2PMo_{12}O_{40}$ after 200 h on stream.

It was already mentioned that on passing from the stoichiometry $PMo_{12}O_{36}$ to $PMo_{14}O_{42}$ phosphorus is unbalanced by a small amount (0.17). We propose that, besides forming the heteropolyanion $(PMo_{14}O_{42})$, thermolysis of the parent $(NH_4)_3PMo_{12}O_{40}$ compound generates some amorphous material, at the expense of a partial structural collapse. This amorphous material would account for the already discussed MoO_x cationic species and also for some small amount of phosphorus oxide, which is likely to be inside the pore system and which could not be located by powder XRD because of its inherent structural disorder.

3.3. Catalytic oxidation of MA to MAA

The catalytic activity and selectivity toward MAA of the different HPAs, after 6 h on stream at 623 K, are reported in Table 4. Significant improvement of catalytic performance is observed for the new cubic anhydride as compared to that of the trigonal anhydrous acid, $H_3PMo_{12}O_{40}$. Since the $(MoO_x)_{0.5}(PMo_{14}O_{42})$ anhydride has some molybdenum ions in an oxidation state lower than 6+, our results strongly suggest that reduced HPAs possess enhanced catalytic activity. For the anhydrous acid, the reduced lifetime on stream was associated [11] with progressive destruction of the initial crystal structure and formation of MoO_3. The same cause is likely to account for the relatively short lifetime of $(MoO_x)_{0.5}(PMo_{14}O_{42})$. Introduction of Cs^+ improves catalytic activity and selectivity, both of which reach the highest values for $Cs(NH_4)_2PMo_{12}O_{40}$, as seen in Table 4.

In agreement with literature data [15,17], our results show that thermal stability of the catalysts can be improved by introducing Cs^+ ions. Table 4 shows that while the lifetime of the catalysts based on the acid form $H_3PMo_{12}O_{40}$ is about 15–30 h, introduction of Cs^+ considerably lengthens this period. The catalyst resulting from $Cs(NH_4)_2PMo_{12}O_{40}$ was found to be fully active after 200 h on stream, and the activity and selectivity of the catalyst based on $Cs_2(NH_4)PMo_{12}O_{40}$

Table 5
Activity and selectivity of the $Cs(NH_4)_2PMo_{12}O_{40}$ catalyst versus time on stream

Time on stream (h)	Conversion (%)	Selectivity MAA (%)
6	63.6	56
80	66	58
140	68.2	58.3
180	68.4	58.5
200	67.5	57.8
270	64.8	56.8
320	63	54

remained unchanged during the whole period of measurements, over 380 h. After this time, the used $Cs_2(NH_4)PMo_{12}O_{40}$ catalyst showed the characteristic deep blue colour of reduced HPAs.

Performance of the most active and selective catalyst, the $Cs(NH_4)_2PMo_{12}O_{40}$ salt, was found to evolve with time on stream as shown in Table 5. Both conversion and selectivity reached maximum values after about 180 h and then declined as time on stream was increased to 320 h.

The observed changes in activity and selectivity of $Cs(NH_4)_2PMo_{12}O_{40}$ upon standing on stream were accompanied by corresponding changes in appearance and XRD patterns (see below). When the used catalyst was inspected it was observed that the typical yellow-greenish color of the original $Cs(NH_4)_2PMo_{12}O_{40}$ salt had changed to dark blue, thus showing that the Keggin anions had undergone reduction. As already mentioned, the reduced polyanion tends to release constitutional water in the temperature range of about 573 to 623 K, forming either an anhydride phase or (depending on temperature) a partially dehydroxylated intermediate species [26,28]. Besides the conspicuous change in color, the used catalyst also showed distinct structural changes which will now be analysed.

3.4. Structural changes of the $Cs(NH_4)_2PMo_{12}O_{40}$ catalyst upon standing on stream

Figure 3 shows some characteristic XRD patterns of the $Cs(NH_4)_2PMo_{12}O_{40}$ catalyst obtained in situ, at 623 K under standard reaction conditions. With increasing time on stream, distinctive changes in the XRD patterns are observed; they include both relative peak intensities and appearance of new diffraction lines. The most conspicuous changes are marked with asterisks (new diffraction lines) and with arrows (intensity changes). Comparison with standard patterns for XRD showed that the new lines come from MoO_3.

More detailed information on the structural changes taking place was obtained from Rietveld analysis of powder diffractograms corresponding to the fresh catalyst and to its evolution products after 20 and 180 h on stream. The results are shown in Table 6, which also gives (for comparison) corresponding data for the same catalyst after 80 h on stream [19]. As time increases, an increasing fraction of extraframework molybdenum atoms (denoted as Mo(2) in Table 6) is observed. At the same time the cubic lattice parameter, a_0, increases form 1.1712 up to 1.1888 nm.

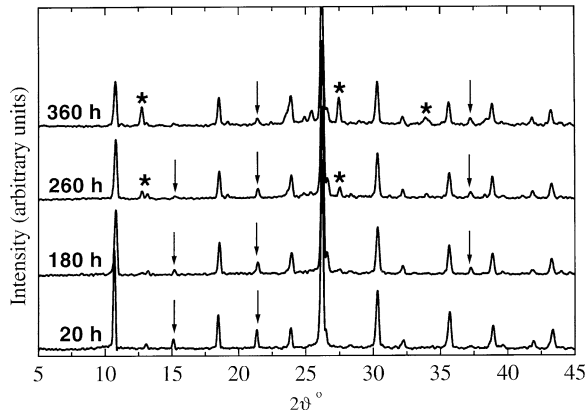

Fig. 3. In situ XRD patterns of $Cs(NH_4)_2PMo_{12}O_{40}$: increasing time on stream from 20 to 360 h. Peaks undergoing the largest relative intensity changes are marked with arrows; asterisks are on peaks corresponding to MoO_3.

Structural analysis (Table 6) strongly suggests that after 20 h on stream, at 623 K, the chemical composition of the catalyst should be close to $Cs(PMo_{13}O_{41})$, according to the corresponding atomic occupancy factors. Since structure analysis is unable to detect any protons which could remain in the sample, the degree of reduction of the original catalyst is not known with certainty, but it has to be at least $2e^-$ per Keggin unit.

The structure of the catalyst after 180 h on stream, short before conspicuous formation of MoO_3 starts, is similar to that of the cubic anhydride depicted in Fig. 2. The two additional molybdenum atoms, denoted as Mo(2) in Table 6, are located at interstitial positions between the polyanions (where the alkali metal cations are usually found), but their atomic coordinates differ significantly from the ideal $\frac{1}{4}$, $\frac{3}{4}$, $\frac{1}{4}$ positions for alkali metal ions in cubic HPA salts. These molybdenum atoms are within bonding distance of the oxygen shell of the Keggin anion, forming the new cesium salt with chemical formula $Cs(PMo_{14}O_{42})$. It is clear from this formula that, in order to keep charge balance, 6 of the 14 molybdenum ions must be in a pentavalent oxidation state.

In general terms, stepwise formation of heteropolyanions having 13 and 14 molybdenum ions with increasing time on stream of $Cs(NH_4)_2PMo_{12}O_{40}$ can be explained by a mechanism similar to that proposed for the formation of the new heteropolyanhydride $(MoO_x)_{0.5}(PMo_{14}O_{42})$, which implies progressive reduction and attendant structural rearrangement of the Keggin units. Completion of this process leads to a six-electron reduction in $Cs(PMo_{14}O_{42})$.

4. Conclusions

The HPA compounds $H_3PMo_{12}O_{40}$, $(MoO_x)_{0.5}(PMo_{14}O_{42})$, $Cs(NH_4)_2PMo_{12}O_{40}$, and $Cs_2(NH_4)PMo_{12}O_{40}$ were tested as catalysts for the oxidative conversion of methacrolein into methacrylic acid at 623 K. The best results were

Table 6
Atomic coordinates and occupancy factors (k) for $Cs(NH_4)_2PMo_{12}O_{40}$ and its transformation products upon standing on stream: S = goodness of fit in the rietveld refinement, a_0 = cubic lattice parameter

Sample	Assymetric unit	x	y	z	k
$Cs(NH_4)_2PMo_{12}O_{40}$ fresh sample[a]	Mo(1)	0.4662	0.4662	0.2585	12
	O(1)	0.3267	0.3267	0.3267	4
	O(2)	0.6517	0.6517	0.0153	12
	O(3)	0.0706	0.0706	0.7627	12
	O(4)	0.1265	0.1265	0.5253	12
	P	0.75	0.75	0.75	1
	Cs	0.25	0.75	0.75	1
	N	0.25	0.75	0.75	2
$Cs(PMo_{13}O_{41})$ 20 h time on stream[b]	Mo(1)	0.4637	0.4637	0.2591	12
	O(1)	0.3240	0.3240	0.3240	4
	O(2)	0.6464	0.6464	0.0018	12
	O(3)	0.0596	0.0596	0.7651	12
	O(4)	0.1320	0.1320	0.5192	12
	P	0.75	0.75	0.75	1
	Mo(2)	0.25	0.6436	0.25	1.05
	O(5)	0.25	0.7965	0.25	1
	Cs	0.25	0.75	0.75	1.03
Formula not given 80 h time on stream[c,d]	Mo(1)	0.4663	0.4663	0.2561	11.42
	O(1)	0.3283	0.3283	0.3283	4
	O(2)	0.6582	0.6582	0.0112	11.45
	O(3)	0.0639	0.0639	0.7736	11.42
	O(4)	0.1301	0.1301	0.5424	11.86
	P	0.75	0.75	0.75	1
	Mo(2)	0.3362	0.7266	0.3362	1.32
	Cs	0.25	0.75	0.75	1
$Cs(PMo_{14}O_{42})$ 180 h time on stream[e]	Mo(1)	0.4693	0.4693	0.2609	12
	O(1)	0.3240	0.3240	0.3240	4
	O(2)	0.6357	0.6357	0.0018	12
	O(3)	0.072	0.072	0.7545	12
	O(4)	0.1345	0.1345	0.5192	12
	P	0.75	0.75	0.75	1
	Mo(2)	0.25	0.6436	0.25	2
	O(5)	0.25	0.79	0.25	2
	Cs	0.25	0.79	0.75	1

[a] $S = 1.26$; $a_0 = 1.1712$ nm.
[b] $S = 1.29$; $a_0 = 1.1830$ nm.
[c] Data taken from Ref. [19].
[d] $S = 1.29$; $a_0 = 1.1843$ nm
[e] $S = 1.25$; $a_0 = 1.1888$ nm.

obtained with the Cs-1 salt $Cs(NH_4)_2PMo_{12}O_{40}$ which, during the catalytic process, showed compositional and structural changes to yield $CsPMo_{14}O_{42}$, which is actually the best catalyst. Structural analysis based on in situ X-ray diffraction patterns have shown that this latter compound has two extraframework molybdenum ions. In situ X-ray diffraction has also shown that conversion of the initial $Cs(NH_4)_2PMo_{12}O_{40}$ compound into the $CsPMo_{14}O_{42}$ phase implies intermediate formation of other phases which progressively evolve when time on stream increases. Structural details concerning these intermediate phases are also given.

$H_3PMo_{12}O_{40}$ and the anhydride $(MoO_x)_{0.5}(PMo_{14}O_{42})$, the structure of which is reported here for the first time, were found to have a short lifetime on stream, about 15 h for the acid and 30 h for the anhydride.

Upon standing on stream, $Cs_2(NH_4)PMo_{12}O_{40}$ gave a catalytic species which showed the largest life time (> 380 h). However, it only gave a 50.7% conversion of methacrolein into methacrylic acid, as compared to 63.7% in the case of the catalyst derived from the Cs-1 salt, and selectivity was also slightly lower in the case of Cs-2 salt.

References

[1] M. Misono, Catal. Rev. Sci. Eng. 29 (1987) 269.
[2] N. Mizuno, M. Misono, Chem. Rev. 98 (1998) 199.
[3] Mitsubishi Rayon, Japanese Patent 1975-23013.
[4] M. Akimoto, K. Shirna, H. Ikeda, E. Echigoya, J. Catal. 86 (1984) 173.
[5] T. Haeberle, G. Emig, Chem. Eng. Technol. 11 (1988) 392.
[6] Ya.G. Popova, T.V. Andrushkevich, Kinet. Katal. 35 (1994) 120.
[7] M.C. Rabia, G. Hervé, S. Launay, M. Fournier, C. Feumi-Jantou, J. Mater. Chem. 2 (1992) 971.
[8] S. Albonetti, F. Cavani, F. Trifirò, M. Gazzano, M. Koutyrev, F.C. Aissi, A. Aboukais, M. Guelton, J. Catal. 146 (1994) 491.
[9] C. Rocchiccioli-Deltcheff, A. Aouissi, M.M. Bettahar, S. Launay, M. Fournier, J. Catal. 164 (1996) 16.
[10] A. Bielanski, A. Malecka, K. Kubelkova, J. Chem. Soc. Faraday Trans. 1 85 (1989) 2847.
[11] T. Ilkenhans, B. Herzog, T. Brown, R. Schlögl, J. Catal. 153 (1995) 275.
[12] V.M. Bondarewa, T.V. Andruskhkevich, R.I. Maximovskaya, L.M. Plyasova, A.V. Ziborov, G.S. Litvak, L.G. Detuseva, Kinet. Katal. 35 (1994) 114.
[13] H.G. Jerschkewitz, A. Alsdorf, H. Fichtner, W. Hanke, G. Öhlmann, Z. Anorg. Chem. 526 (1985) 73.
[14] E. Payen, S. Kasztelan, J.B. Moffat, J. Chem. Soc. Faraday Trans. 88 (1992) 2263.
[15] N. Mizuno, T. Watanabe, M. Misono, Bull. Chem. Soc. Jpn. 64 (1991) 243.
[16] L.M. Deußer, J.W. Gaube, F.G. Martin, H. Hibst, Stud. Surf. Sci. Catal. 101 (1996) 981.
[17] Sumitomo Kagaku Kogyo K. K., Japanese Patent JP 04063139 A2, 1992.
[18] L. Marosi, G. Cox, A. Tenten, H. Hibst, J. Catal. 194 (2000) 140.
[19] L. Marosi, G. Cox, A. Tenten, H. Hibst, Catal. Lett. 67 (2000) 193.
[20] L. Marosi, E. Escalona Platero, J. Cifre, C. Otero Areán, J. Mater. Chem. 10 (2000) 1949.
[21] Sumitomo Chemical Company, US Patent 4,565,801, 1986.
[22] S. Brendt, D. Herein, F. Zemlin, E. Beckmann, G. Weinberg, J. Shütze, G. Mestl, R. Schlögl, Ber. Bunsenges. Phys. Chem. 102 (1998) 763.
[23] C. Machal-Roch, N. Laronze, N. Guillou, A. Tézé, G. Hervé, Appl. Catal. 203 (2000) 143.
[24] N.N. Greenwood, A. Earnshaw, Chemistry of the Elements, Pergamon, Oxford, 1984.
[25] L.C. Josefowicz, H.G. Karge, E. Vasilyeva, J.B. Moffat, Micropor. Mater. 1 (1993) 313.
[26] A. Bielansky, A. Cichowlas, D. Kostrzewa, A. Malecka, Z. Phys. Chem. N. F. 167 (1990) 93.
[27] J.C.A. Boeyens, J.G. McDougal, J. Van R. Smith, J. Solid State Chem. 18 (1976) 191.
[28] W. Yong, X. Quan, J. Zheng, Thermochim. Acta 111 (1987) 325.
[29] R.A. Young, The Rietveld Method, Oxford Univ. Press, Oxford, 1993.
[30] T. Ilkenhans, H. Siegert, R. Schlögl, Catal. Today 32 (1996) 333.
[31] C. Marchal-Roch, R. Bayer, J.F. Moisan, A. Tézé, G. Hervé, Top. Catal. 3 (1996) 407.
[32] C. Marchal-Roch, N. Laronze, N. Guillou, A. Tézé, G. Hervé, Appl. Catal. 199 (2000) 33.